International Journal of Heat and Mass Transfer 52 (2009) 3235–3249

Contents lists available at ScienceDirect

International Journal of Heat and Mass Transfer

journal homepage: www.elsevier.com/locate/ijhmt

Study of the critical heat flux condition with water and R-123 during flow boiling in microtubes. Part I: Experimental results and discussion of parametric effects

A.P. Roday, M.K. Jensen *

Department of Mechanical, Aerospace and Nuclear Engineering, Rensselaer Polytechnic Institute, Troy, NY 12180-3590, USA

ARTICLE INFO

Available online 9 March 2009

Keywords:
CHF
Boiling
Water
R-123
Flow pattern
Quality
Subcooled
Saturated
Microtube

ABSTRACT

Extensive experimentation was performed to obtain flow boiling critical heat flux data in single stainless steel microtubes with diameters from 0.286 to 0.700 mm over a wide range of mass fluxes, inlet subcoolings, and exit pressures for two different working fluids (water and R-123). The effect of different operating parameters – mass flux, inlet subcooling, exit quality, heated length and diameter – were assessed in detail (Part I of the paper). The conventional DNB-type behavior is observed in the high subcooled region, and the typical dryout type behavior is seen in the high-quality saturated region when the flow is completely annular. The flow in transitional flow patterns (churn–annular or slug–annular) causes a peculiar increase of CHF with exit quality. Also, the increased void fraction near the saturated region in subcooled boiling results in increased subcooled CHF values. Part II of the paper deals with comparison of data with existing correlations and development of a new correlation to predict the CHF condition in the subcooled liquid region.

1. Introduction

In heat transfer engineering, the thermal management of electronic devices has become challenging due to the continuous and rapid development of integrated circuit technology. With the increased packaging density and performance of microelectronic devices, IC chip power has significantly risen in the last two decades. This imposes a practical limit on traditional cooling approaches such as natural and forced convection using air. The use of two-phase cooling has many attractive features from a thermal perspective, such as reduced volume requirements when removing large amounts of heat and operating with lower temperature differences. In contrast to the above heat flux controlled applications, in modern wall temperature controlled situations, with the development of nanotechnology and fuel-cell technology, more compact and enhanced heat exchangers are being designed. Ultra-compact heat exchangers typically have surface area densities as high as 10,000 m^2/m^3 [1]. Both of the above applications are characterized by channels having dimensions in the 100–1000 μm range. During flow boiling, the critical heat flux (CHF) condition sets an upper limit on the heat transfer and this should be understood well to design efficient micron-sized heat transfer devices.

There are few investigations of CHF studies in microchannels and mini/micro circular tubes. There have been some studies in tubes with smaller dimensions (up to about 0.3-mm) involving very high mass velocities intended for extremely high heat flux removal as in fusion reactors [2,3]. Celata et al. [4] have conducted subcooled CHF studies in tube diameters as small as 0.25 mm, but these were, again, for very high heat fluxes (up to 70 MW/m^2) and high mass fluxes (greater than 5000 kg/m^2s) in the fusion technology application. Studies at lower mass fluxes, intended for applications as mentioned above, are limited. Nariai et al. [5] reported CHF studies with water at ambient exit pressure in stainless steel tubes with inside diameter of 1-mm; tests were performed from the subcooled to the quality region (very close to zero quality) for high mass fluxes ranging from 7000 to 11,000 kg/m^2s. They indicated that the CHF decreased with an increase in exit quality in the subcooled region. It has a minimum in this region very close to zero quality. As quality was further increased to a positive value the CHF increased sharply and, thereafter, had a decreasing trend with increases in quality. The maximum exit quality in their data was 0.05. A similar trend was observed by Bergles et al. [6] for CHF with deionized water in a stainless steel 2.38-mm tube with L/d = 15, mass flux of 3000 kg/m^2s, and an exit pressure of 207 kPa.

Roach et al. [7] studied the CHF associated with flow boiling of subcooled water in circular tubes with diameters of 1.17-mm (L/d = 137) and 1.45-mm (L/d = 110), mass velocities from 250 to 1000 kg/m^2s, exit pressures from 344 to 1043 kPa, and inlet temperatures from 49 to 72 °C. They observed the CHF condition at very high exit qualities (around 0.8) indicating dryout. They found that in both the tube sizes for pressure around 100 psi and mass flux about 800 kg/m^2s, CHF did not occur at all, and a smooth transition from nucleate to film boiling took place.

* Corresponding author.
E-mail address: JenseM@rpi.edu (M.K. Jensen).

0017-9310/$ - see front matter © 2009 Elsevier Ltd. All rights reserved.
doi:10.1016/j.ijheatmasstransfer.2009.02.003

Nomenclature

G	mass flux, kg/m^{2}s
J	superficial velocity, m/s
L	length of the tube, mm
Nu	Nusselt number
P	Pressure, kPa
Pr	Prandtl number
Q	volumetric flow rate, m^3/s
Re	Reynolds number
T	temperature, °C
We	Weber number
d	diameter, mm
h	specific enthalpy, J/kg
x	quality

Greek letters

ΔT	temperature difference, °C
Δp	pressure difference, Pa
ρ	density, kg/m^3
σ	surface tension, N/m
δ	axial location, mm

Subscripts

T	total
TS	test section
c	critical
d	diameter
$exit$	at exit
f	liquid
fg	liquid–vapor
g	vapor
h	heated
i	inlet
in	inside, tube
o	outlet
out	outside, tube
sat	saturation
sh	shunt
sub	subcooling, inlet
w	wall

CHF experiments were performed by Lazarek and Black [8] with R-113 in a stainless steel tube of inside diameter 3.15-mm (L/d = 40) in a vertical orientation. The mass velocities were in the range of 140–740 kg/m^{2}s. Inlet subcooling varied between 3 and 73 °C. They found that the CHF occurred at very high exit qualities (from 0.5 to 0.8). Following the power increase, the wall temperatures underwent progressively large oscillations due to intermittent rewetting of the passage wall. CHF occurred at the exit of the heated test section.

Qu and Mudawar [9] measured the CHF for a water-cooled microchannel heat sink which contained 21 parallel 215 × 821 μm channels. The tests were conducted with deionized water over a mass velocity range of 86–368 kg/m^{2}s, inlet temperatures of 30 and 60 °C, and outlet pressure of 113 kPa. CHF was found to increase with the increase in mass velocity, but virtually independent of inlet temperature.

Yu et al. [10] carried out CHF experiments with water in a stainless steel 2.98-mm inside diameter tubing (L_h/d = 305) and a pressure of about 200 kPa. The outside diameter of the test section was 4.76-mm. CHF was found to decrease with a decrease in mass flux (mass fluxes varied between 50 and 200 kg/m^{2}s). CHF qualities were found to be relatively high, above 0.5. Lezzi et al. [11] reported experimental results on CHF in forced convection boiling of water in a horizontal tube of diameter 1-mm and L/d = 250, 500, and 1000. The mass flux was varied between 800 and 2700 kg/m^{2}s. In all the cases the quality at the outlet was high (greater than 0.6), and the critical heat flux was reached through dryout.

Jiang et al. [12] conducted CHF studies with water with an array of microchannels of either 35 or 58 channels each of 40-μm hydraulic diameter and either 10 or 34 channels of 80-μm hydraulic diameter. In all the tested devices, the wall temperature increased almost linearly with heat flux until the onset of CHF condition was developed. They concluded that due to the microscale size of the channels, a stable vapor core was established in the microchannel at an early stage such that the evaporation at the liquid film–vapor core interface became the dominant heat transfer mechanism. The typical bubbly flow where the bubbles form, grow, and detach from the channel wall was suppressed.

Recently, Wojtan et al. [13] investigated saturated critical heat flux with R-134a and R-245fa in a single uniformly heated microchannel of 0.5 and 0.8 mm internal diameter. They did not find any influence of inlet subcooling on CHF, but at the same time they found the CHF to decrease with an increase in exit quality; however, the range of inlet subcooling considered was very limited ranging from 4.5 to 12 °C.

Flow instabilities can severely affect the tests conducted to determine the CHF condition, and instabilities need to be addressed when performing the CHF experiments. With the absence of an upstream throttle valve, as in studies by Jiang et al. [12], the compressible volume instability could be likely responsible for a reduced CHF value. Qu and Mudawar [9] took care to address this instability by installing a throttle valve upstream of the heat sink and found that severe flow oscillations occurred when the valve was open; by throttling this valve, the oscillations were virtually eliminated. However, Qu and Mudawar observed an unusual phenomenon as CHF approached; there was a vapor backflow from all the channels towards the inlet plenum and this was responsible for the lack of inlet subcooling effect seen in the CHF data as mentioned previously. In case of single microchannels, this can be taken care of by having a very high upstream pressure drop as is seen in the studies described in a subsequent section by Roday et al. [14]. In the case of parallel microchannels, improved fabrication techniques can be used to employ flow restrictions at the inlet of each channel to accomplish the pressure drop needed [15] and, thus, avoid excursive instabilities observed by Qu and Mudawar. This technique was used by Koşar et al. [16], who employed inlet restrictors to study the suppression of flow boiling oscillations in a silicon microchannel device having five channels of size 200-μm wide and 264-μm deep, 1 cm long. Using the same device, Koşar and Peles [17] studied the CHF condition of R-123 at exit pressures ranging from 227 to 520 kPa. CHF data were obtained over heat fluxes from 53 to 196 W/cm^2 and mass fluxes from 291 to 1118 kg/m^{2}s. Flow images and high exit qualities suggested that dryout was the leading CHF mechanism. CHF increased fairly linearly with mass flux. Kuan and Kandlikar [18] studied the effect of flow boiling stability on CHF with R-123 in six parallel microchannels of hydraulic diameter 546.5-μm (cross-sectional area of each microchannel is 1054-μm × 157-μm) machined on a copper block

of dimensions 88.9 mm × 29.6 mm by using pressure drop elements (PDE) which were expected to help reduce vapor backflow; however, no visual flow patterns were reported. They developed a theoretical model to represent the CHF mechanism and correlated it with their experimental data. Their results show a decrease in the CHF value with the use of restrictors which is contrary to what is expected. Since the actual design of the restrictors is not well described, the reasons for this behavior are not clear. Better design of the restrictors is needed to control this instability as in the study of Koşar et al. [16], who used microfabricated orifices which were a part of the microchannel device.

The CHF condition has received much less attention than the boiling heat transfer coefficient. The studies dealing with CHF in small diameter tubes for low mass fluxes are limited although there have been studies in small tube diameters down to about 0.3 mm, but such studies involved very high mass fluxes [3]. The data available for tubes are those for flow boiling of R-113 and water. There are few data for any of the hydro chlorofluorocarbons (HCFCs). There are few studies for CHF at sub-atmospheric pressures or studies close to ambient pressure with low mass fluxes. There are not enough data to analyze the effect of the different variables (such as mass flux, pressure, exit quality, tube diameter) on the CHF condition.

There are numerous discrepancies in the existing data about the CHF condition. Thus, there is no general agreement on the mini/microchannel CHF studies conducted so far. For example, in minichannels, Roach et al. [7] found the CHF to increase with increasing channel diameter, but Bergles et al. [6] found an inverse dependence of diameter on CHF. Oh and Englert [19] found a weak linear relationship between inlet subcooling and CHF, but Bowers and Mudawar [20] found that the CHF was not at all affected by the inlet subcooling during their studies in parallel microchannels. Wojtan et al. [13] also found, in their studies with single tubes, that the CHF was not dependent on inlet subcooling. The data by Yu et al. [10] indicated that the CHF increased with an increase in exit quality, but the Wojtan et al. [13] data depicts the opposite effect. The CHF studies by Roach et al. [7] shows that the CHF increases with increasing pressure, but the data in some studies [13] do not show a strong dependence of pressure on CHF. Many researchers have attempted to predict their data with existing correlations, but with mixed results. Many different correlations have been developed, but they are mostly applicable to the limited data range over which the experiments were conducted. Conjugate heat transfer effects have been neglected, and the effect of flow instabilities have not been investigated properly during some of the experiments. The effects of axial conduction through the tube walls or through the blocks on which the channels are machined can significantly alter the CHF condition. Most of the experiments have ignored this aspect. Likewise, flow oscillations can have a significant negative effect on the CHF condition. Generally, flow distribution in parallel channels tends to be non-uniform. Since the CHF condition is dependent on flow rate, most of the data from the experiments using parallel channels are not reliable as the flow rate through the individual channels is not exactly known. The current literature on CHF in microchannels is not sufficient to predict the boiling crisis over the range of parameters typically encountered in applications where such small-size channels find potential use. Likewise, there is a clear lack of accurate and validated models to predict two-phase heat transfer characteristics. Thus, the objectives of the present study are:

- To gain a better understanding of the CHF condition in microchannels, so that the CHF condition can be predicted with confidence over a wide range of operating parameters such as channel material, type of fluid, geometrical sizes, mass fluxes, operating pressures and inlet subcoolings.
- To understand the impact of flow oscillations on the critical heat flux condition.
- To determine the flow patterns from the experimental CHF data using existing flow pattern maps/models.
- To assess the capability of using existing correlations for conventionally sized channels and available correlations for microchannels to predict the onset of the critical condition in microchannels and develop new correlations if needed (Part II of the paper).

2. Experimental apparatus and procedures

For the CHF experiments, a flow loop was designed and constructed to obtain experimental data on the CHF condition over a wide range of operating conditions [refer Table 1(a) and (b)]. The flow loops used for testing water and R-123 were identical, except that the equipment used on the refrigerant set-up was selected to be compatible with R-123. A schematic of the flow loop used for testing is shown in Fig. 1.

The major components of the loop are a storage tank, flowmeters, and the test section assembly. The tank was equipped so that the pressure could be varied from a vacuum to a pressure of 5 bars; likewise, it was used to degas the fluids. As a safety measure, a pressure relief valve was also provided on the tank.

Fluid was circulated in the loop by imposing a pressure difference between the two tanks. The fluid was heated to the desired temperature by passing it through a 200-mm long preheater section. The preheated fluid was throttled before it entered the test section. The throttling valve controlled the inlet condition of the fluid to the test section and reduced flow instabilities during boiling. The preheated fluid then flowed through the test section. (A detailed discussion of the test section and its mounting is provided below.) A differential pressure transducer measured the pressure drop across the test section length. A Bourdon-type pressure gauge recorded the pressure at the exit of the test section. Following the test section, the fluid entered Tank B from where it was later pumped back to the main storage Tank A.

The test sections used for obtaining boiling heat transfer and CHF data were made from individual hypodermic tubing having a circular geometry. The diameter of each test section used in the experiment was carefully measured using an optical microscope having a measuring probe attachment. The test section was heated by passing DC power through it. The test section was enclosed by a guard heater to minimize heat losses during diabatic experiments as shown in Fig. 2. A 2.0-cm thick layer of insulation was wrapped around the test section. A 5-cm diameter copper tube, with resistance wire and a thermocouple bonded to it, was secured over this insulation. Then another 3-cm layer of insulation was wrapped around the copper tube. The guard heater covered the area from compression fitting to compression fitting. The power to this guard heater was controlled through a variable transformer.

An automatic test section power shut-off circuit was used to prevent test section damage at CHF. The switching time of the relay is about 7 ms. Once the test section assembly was completed, T-type thermocouples (copper–constantan) were bonded to the test section at different axial locations using a high-temperature epoxy. Thermocouples nearer to the exit of the heated section were spaced close to each other (about 2.0 mm apart) to better track the CHF condition. Also, one thermocouple was mounted on the test section ahead of the heated length to check for any backflow of vapor and axial conduction away from the heated section. Pressure taps were provided at the two ends of the test section (about

Table 1
Experimental conditions for water and R-123 CHF experiments.

Parameter	Test section – A	Test section – B	Test section – C
(a) CHF data – water			
d_{in} (mm)	0.286	0.427	0.700
d_{out} (mm)	0.450	0.550	1.060
L_h (mm)	21.66, 39.82, 57.62	59.00	70.70, 96.0
L_T (mm)	138.65	121.96	138.07
G (kg/m^{2}s)	320, 1570	315, 560, 870, 1570	315, 560
P_{exit} (kPa)	26, 102	25.3, 102, 179	102
ΔT_{sub} (°C)	5–80[a]	2–50	2–80
	Test section – D	Test section – E	Test section – F
(b) CHF data – R-123			
d_{in} (mm)	0.286	0.430	0.700
d_{out} (mm)	0.450	0.550	1.060
L_h (mm)	17.26, 37.13, 58.91	25.37, 55.47	39.72, 90.84
L_T (mm)	136.20	141.70	138.07
G (kg/m^{2}s)	375, 530, 825	375, 530, 825	375, 530, 825
P_{exit} (kPa)	165, 225[b]	168	168
ΔT_{sub} (°C)	2–25[a]	2–17	2–15

[a] The range depends on exit pressure.
[b] For the pressure of 225 kPa the heated lengths were 17.26 and 58.91 mm.

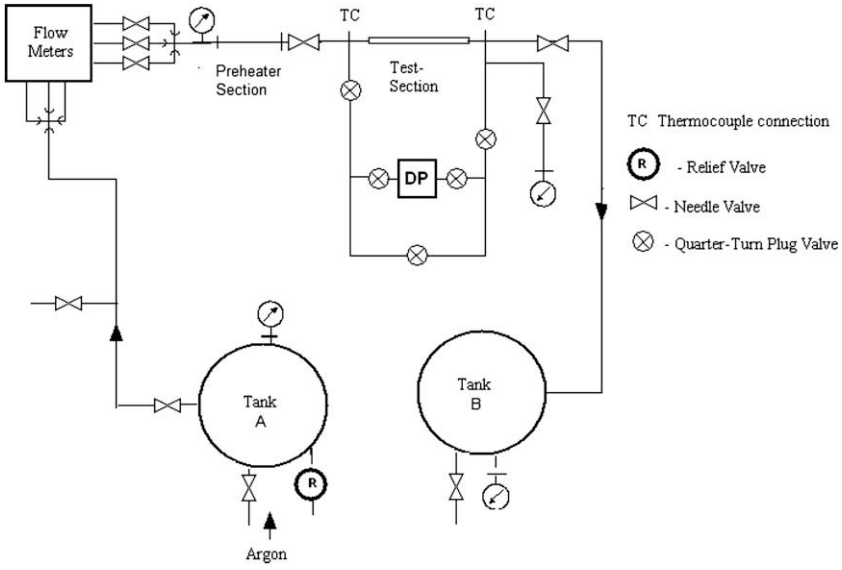

Fig. 1. Schematic of the flow loop.

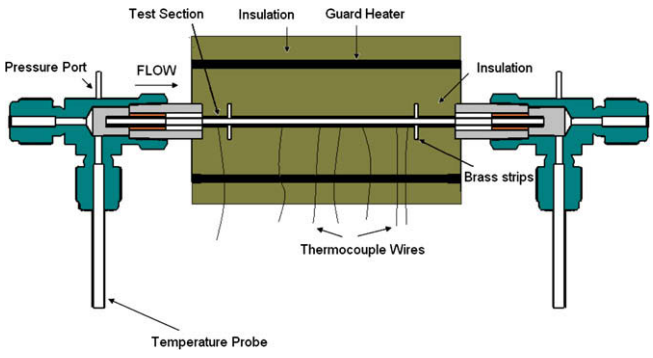

Fig. 2. Test section assembly.

35 mm away from the heated section). Temperature probes measured the temperature of the working fluid at the inlet and exit of the test sections at the same locations as the pressure taps. The inlet and exit portions of the test section were heavily insulated to avoid heat loss.

Calibration of the flowmeters was done using the weigh tank technique of measuring the volume of fluid collected in a given amount of time. Calibration of the Bourdon-type pressure gauges was done using a deadweight tester. The differential pressure transducers were calibrated for each diaphragm using a water column over the full pressure range of the transducers for the lower differential pressure ranges and with deadweight tester for the higher differential pressure range.

The fluid was degassed before circulating in the loop. This was done by passing high pressure argon through the water stored in the Tank A. This gas stripped the dissolved oxygen from the fluid. The process was carried out in vacuum (about 50 kPa) so that dissolved gases along with the argon were removed from the tank, thus leaving the tank with degassed water.

For an experimental run, the flow was set to the desired value by adjusting the in-line valves. The exit pressure was set by controlling the pressure in Tank B. The preheater and guard heater were turned on and set to the desired values. A criterion of a maximum ±0.5 °C variation in wall temperatures in about 15 min was set to detect the quasi-steady state as the wall temperatures remained fairly constant after about 15 min indicating that a steady

state was attained. It took up to about 2 h to reach the initial quasi-steady state depending on the operating conditions, and about 30 min for each new setting of the flow rate. For every new setting of the inlet temperature, it took another 1 h for the flow to reach steady state. Once steady state was reached, data were recorded of those operating conditions.

A single-phase experiment was first performed, and the heat loss was estimated by comparing the sensible heat gained by the water (inlet and outlet water temperatures were measured during the experiment) with the power input to the test section. This experiment was done by setting the power to the test section at a particular value, and adjusting the guard heater power so that the guard heater temperature was only slightly above the wall temperature on the test section. This ensured minimum heat loss from the test section wall. The measurements of flow, temperature, and voltages were then recorded.

Next, the guard heater temperature was set close to the saturation temperature (corresponding to the outlet pressure). The inlet fluid temperature was again set to the desired value, steady state was reached, and then the power to the test section was increased in progressively smaller increments until the CHF condition was reached. This condition was marked by a nearly instantaneous rise in the wall temperature of about 80–100 °C over the saturation temperature.

3. Data reduction

The measured quantities were the total pressure drop ($\Delta p_{T\text{-}expt}$) from the differential pressure transducer, the volumetric flow rate (Q) from the flowmeter, the test section inside diameter (d_{in}), the test section length (L), the voltage across the shunt (V_{sh}), voltage across the test section (V_{TS}), heated length of the test section (L_h), fluid inlet temperature ($T_{f,i}$), fluid exit temperature ($T_{f,o}$), the wall temperatures ($T_{w,o,\delta}$), and the exit pressure (P_{exit}). The derived quantities included mass flow rate, mass flux, Reynolds number, heat flux, Nusselt number, and quality. An energy balance was used to calculate local fluid conditions in the test section; CHF conditions were identified at the last thermocouple location. Heat loss from the test section was estimated by calibration of the system; the guard heater ensured a heat loss of less than ±5% of test section power. Total pressure drop was calculated including entrance and exit losses and frictional losses (developing region and fully developed region). The thermophysical and the thermodynamic properties of water and R-123 were obtained using Engineering Equation Solver (EES). An uncertainty analysis was performed using the method suggested by Kline and McClintock [21] for the propagation of error, and uncertainties (depending on test section diameter) were estimated to be: mass flux, ±2.1–2.7%; Reynolds number, ±2.1–2.8%; heat flux, ±5%; Nusselt number, ±5.3–5.5%; quality, ±5.8%. The details of the data reduction and uncertainty analysis are described in Roday [22].

4. Experimental results

Following the procedures outlined, the CHF condition was experimentally investigated in stainless steel microtubes of various diameters (d_{in}) for water and R-123 over a range of mass fluxes, inlet subcoolings and exit pressures (see Table 1). A total of about 225 CHF data points were obtained during this study.

A comparison between the properties of R-123 and water based on their respective experimental conditions (from Table 1) is provided in Table 2.

Table 2
Property comparison for R-123 and water.

Property	R-123	Water
ρ_f/ρ_g	101–138	930–6022
σ (N/m)	0.012–0.013	0.056–0.065
h_{gf} (kJ/kg)	160–165	2211–2343
We_d	2–25	0.5–20
P_c (kPa)	3668	22064
P_{exit}/P_c	0.045–0.061	0.001–0.008

4.1. Single-phase pressure drop and heat transfer – water and R-123

Single-phase studies were conducted in the test sections before running CHF experiments. The experimental pressure drops were close (within ±10%) to that calculated from correlations for most of the data over Re up to 1100 for all the test sections. Fig. 3 shows this agreement for d_{in} = 0.286, 0.427, and 0.700 mm for studies conducted with water.

During the single-phase heat transfer experiments, the flow was hydrodynamically fully developed but was thermally developing for parts or all of the test section heated length. The heat transfer results were compared with the modified Hausen correlation (for constant heat flux) given below.

$$Nu = 4.36 + \frac{0.19(RePrd_{in}/L)^{0.8}}{1 + 0.117(RePrd_{in}/L)^{0.467}} \quad (1)$$

This correlation overpredicted the data at lower Reynolds number and underpredicted them at higher Re for all the three diameters. As seen in Fig. 4, the deviation for d_{in} = 0.427 mm [Test section B, Table 1(a)] is about −75% at lower Reynolds number ($Re \sim 50$) and 25% at $Re \sim 900$. The data for the other two diameters were qualitatively similar. These laminar single-phase heat transfer results are consistent with other results from the literature [23,24].

Most of the studies on single-phase flow in microchannels were able to measure pressure drop characteristics which were consistent with conventional sized channels but showed marked deviations in heat transfer characteristics [25], similar to what we have observed. A definite reason for this disagreement in microchannels is not yet known. Single-phase pressure drop and heat transfer experiments were performed before the CHF experiments were carried out for R-123 as well. Results show fairly good agreement of pressure drop predictions, but the Nusselt Number was underpredicted at low Re and overpredicted at high Re similar to that observed in experiments conducted with water.

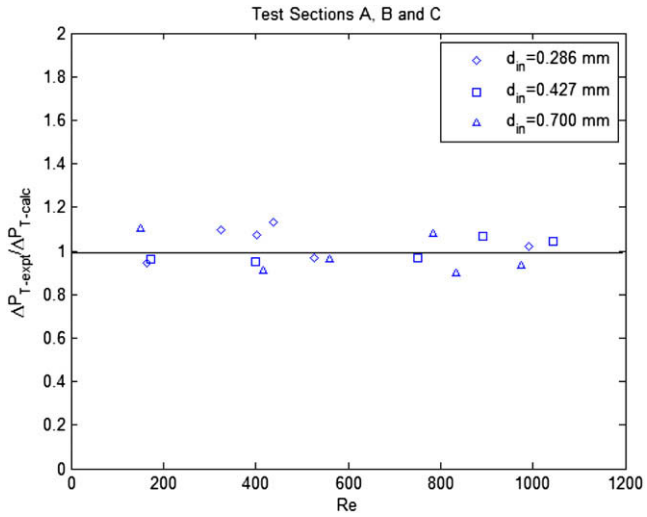

Fig. 3. $\Delta p_{T\text{-}expt}/\Delta p_{T\text{-}calc}$ versus Re for d_{in} = 0.286, 0.427, and 0.700 mm.

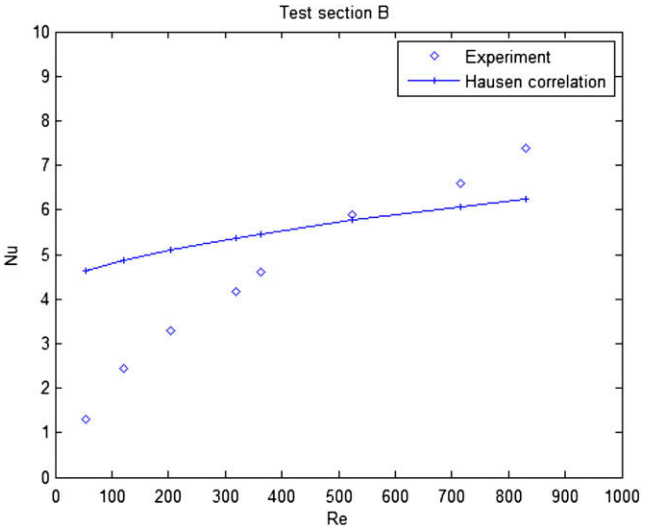

Fig. 4. Comparison of experimental Nusselt number with modified Hausen correlation, d_{in} = 0.427 mm.

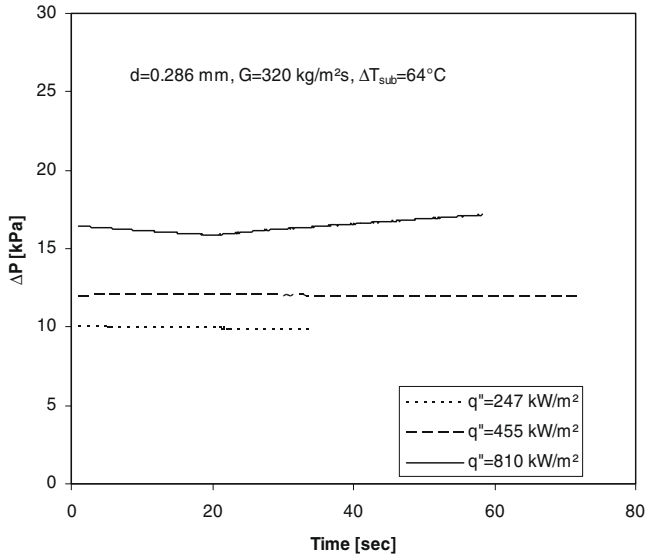

Fig. 6. Pressure drop versus time for water; G = 320 kg/m^{2}s, ΔT_{sub} = 64 °C, d_{in} = 0.286 mm.

4.2. Critical heat flux (CHF) studies

In the two-phase study, there were about 140 CHF data points with water and 85 for R-123. There are some additional data points where the characteristic sharp rise in wall temperature associated with the CHF condition was not observed. All the data are tabulated in Roday [22]. Before discussing the results for each of the three diameter tubes, the flow conditions during these experiments are described and plots of typical wall temperature variations with heat flux are depicted in the next sub-section.

Flow was stabilized during the CHF experiments by maintaining a very high pressure drop (130–200 kPa) upstream of the test section through use of an inlet throttle valve; the rotameter float position was constant. A thermocouple mounted on the test section wall just before the heated section did not show any appreciable variations in temperature (the temperature was very close to the inlet water temperature), which indicated that there was no backflow of vapor or axial conduction outwards from the heated section. The pressure drop showed only small fluctuations with time (single-phase and two-phase flow regimes) except for very close to the CHF condition. One such plot of pressure drop versus time for d_{in} = 0.427 mm, at sub-atmospheric pressure and a mass flow rate of 560 kg/m^{2}s for water, is shown in Fig. 5. Pressure drop fluctuations for d_{in} = 0.286 mm are depicted in Fig. 6. The magnitudes of the fluctuations in Figs. 5 and 6 were typical of all tests.

For the flow boiling tests (water and R-123), there was a characteristic sharp rise in wall temperature at the point of CHF, as can be seen in the plot of wall superheat versus heat flux depicted in Fig. 7 for water CHF data and Fig. 8 for R-123. Note, also, that prior to the initiation of the CHF condition, often the wall temperature initially jumped up by about 35 °C, then dropped back; with further increases in heat flux, the CHF condition was reached (wall temperature was approximately 165 °C). At this point, test section power was automatically shut-off to prevent test section damage. A similar observation was made in other tests with lower mass fluxes where the steady increase in heat flux caused the wall temperatures to increase by about 40–50 °C and then fall back before finally attaining the CHF condition. The jumps in the wall temperature just prior to CHF could be due to the occurrence of dry patches on the tube wall and when the liquid occasionally rewetted the wall, the temperatures would fall back. CHF would occur

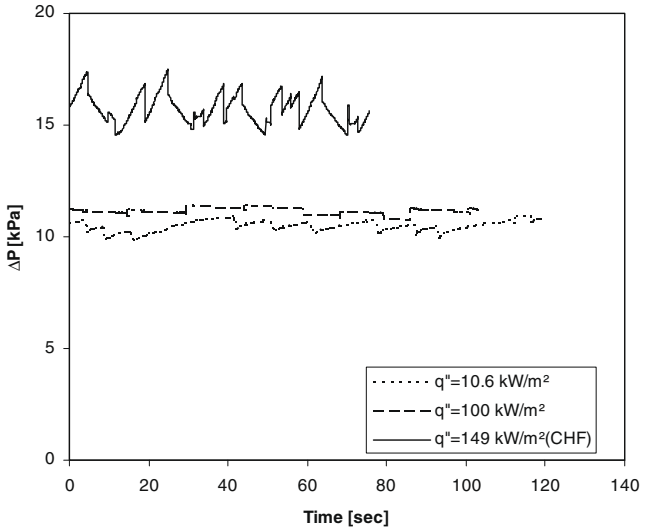

Fig. 5. Pressure drop versus time for water; G = 560 kg/m^{2}s, ΔT_{sub} = 38 °C, P_{exit} = 25 kPa, d_{in} = 0.427 mm.

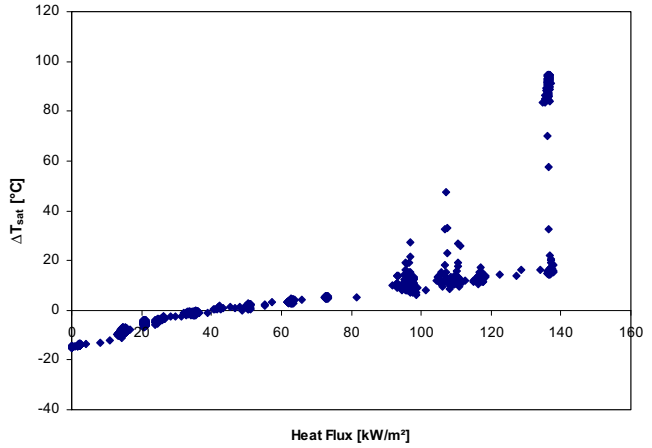

Fig. 7. Wall superheat versus heat flux for water (P_{exit} = 25 kPa; G = 315 kg/m^{2}s; ΔT_{sub} = 15 °C, d_{in} = 0.427 mm).

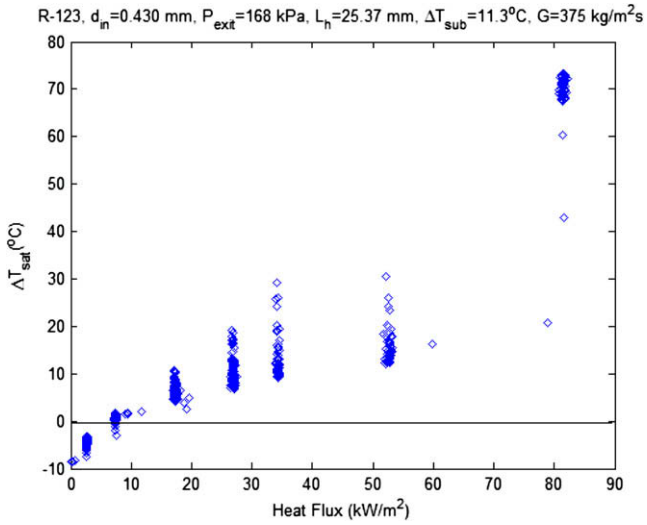

Fig. 8. Wall superheat versus heat flux for R-123 (d_{in} = 0.430 mm, ΔT_{sub} = 11.3 °C, G = 375 kg/m^{2}s, L_h = 25.37 mm).

near the exit when the tube wall became completely dry. Lazarek and Black [8] observed a similar wall temperature response during CHF tests in a 3.1 mm diameter tube at mass flux of about 270 kg/m^{2}s.

The characteristic CHF did not occur for some of the water CHF experiments up to high heat fluxes, at which point power was shut down so that the test sections were not destroyed. This happened for some of the tests carried out at low values of inlet subcooling (ΔT_{sub} = 2–7 °C). The wall temperature kept linearly increasing as the heat flux was increased. When the wall superheats reached a relatively high value (40–60 °C), the experiment was stopped before the CHF was observed to save the test section. For this reason, very few saturated CHF data points could be obtained.

4.3. Parametric effects on CHF

4.3.1. Effect of mass flux on CHF

Fig. 9 depicts the dependence of CHF on mass flux for the tube diameter of 0.286 mm. The subcooled CHF data were compared at

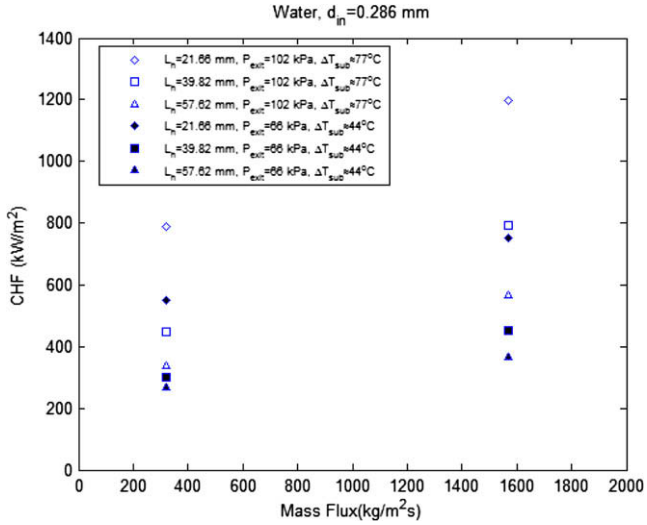

Fig. 9. Effect of mass flux on CHF for d_{in} = 0.286 mm with water.

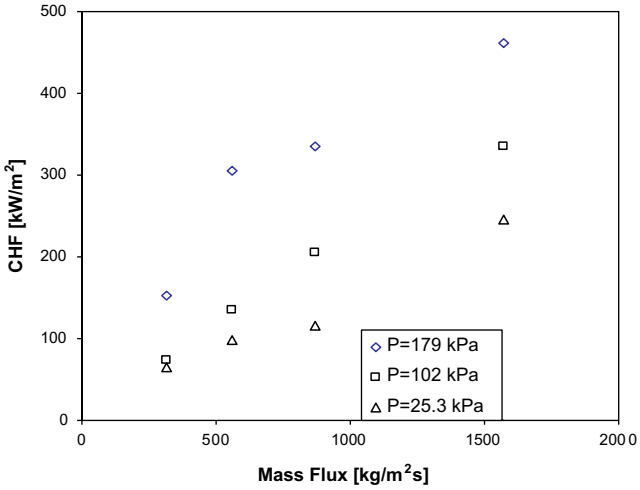

Fig. 10. Effect of mass flux on CHF for d_{in} = 0.427 mm with water.

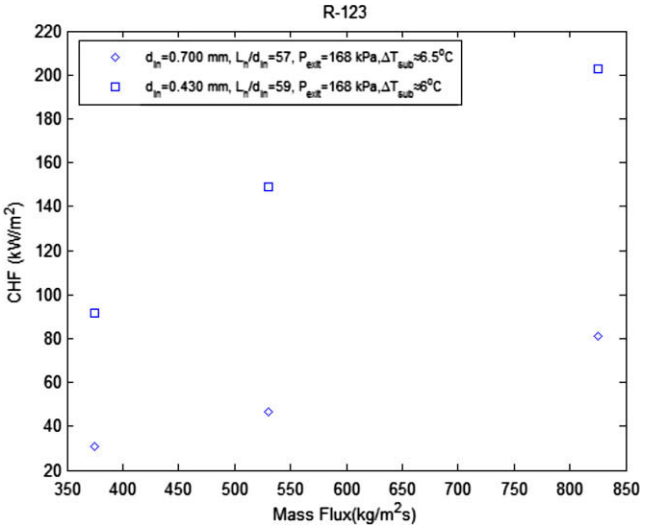

Fig. 11. Effect of mass flux on CHF for R-123, d_{in} = 0.430 and 0.700 mm.

about a fixed value of inlet subcooling. It is seen that for the two exit pressures (P_{exit} = 102 and 66 kPa), the CHF increased with mass flux for all the three heated lengths. A similar mass flux effect is observed in tests conducted with d_{in} = 0.700 and 0.427 mm. The results for the CHF dependence on mass flux for four different mass flux values in 0.427 mm diameter tube are depicted in Fig. 10.

For R-123, the CHF increases with an increase in mass flux at a given value of inlet subcooling. Fig. 11 shows that CHF increases with mass flux for both the tube diameters d_{in} = 0.430 mm and 0.700 mm. A similar mass flux effect is observed for d_{in} = 0.286 mm.

A similar mass flux dependence of CHF has been observed by other researchers such as for water at reduced pressures through parallel microchannels of 0.227 mm hydraulic diameter [26], and for flow of R-134a through single stainless steel tubes of 0.5 and 0.8 mm inside diameter [13]. Thus, an increasing CHF with mass flux is seen in studies with different fluids. However, the water data of Kosar et al. and the data shown here have a major difference. The Kosar et al. data have significantly higher CHFs – perhaps due to a smaller hydraulic diameter or conjugate heat transfer effects since their experiments were multiple parallel channels in a high conductivity block (Si).

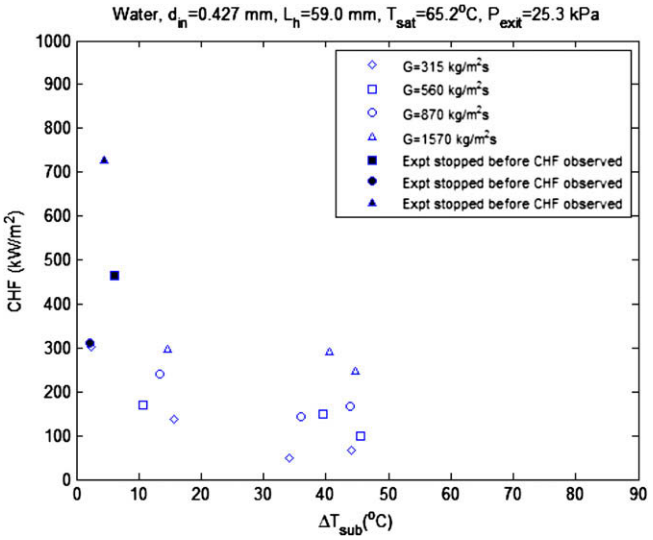

Fig. 12. Effect of inlet subcooling on CHF for d_{in} = 0.427 mm and P_{exit} = 25.3 kPa.

4.3.2. Effect of inlet subcooling and exit quality

The effect of inlet subcooling on CHF for d_{in} = 0.427 mm is shown in Fig. 12 at different mass fluxes. It seems, from the limited data that could be obtained at higher subcoolings, that the CHF slightly decreased with a decrease in inlet subcooling for critical qualities further away from the saturated liquid point, which is similar to conventional tubes but the number of data points are not enough to prove it conclusively. From Fig. 12, the slight decrease at higher subcoolings is more evident for G = 315 and 870 kg/m^{2}s where the critical qualities are about −0.40 when compared to the other data (G = 560 and 1570 kg/m^{2}s) where this trend seems to be missing as the critical qualities were only about −0.25. At lower subcoolings (water inlet temperature close to the saturation temperature), the CHF increased with a decrease in subcooling. This trend was observed at all exit pressures. For the cases where the CHF dramatically increased with reduction in inlet subcooling, the exit quality at CHF was close to zero. With further decrease in inlet subcooling ($\Delta T_{sub} \sim$ 2–4 °C), the wall temperature kept linearly increasing with heat flux and, as previously mentioned, the experiment had to be stopped before the CHF condition was observed.

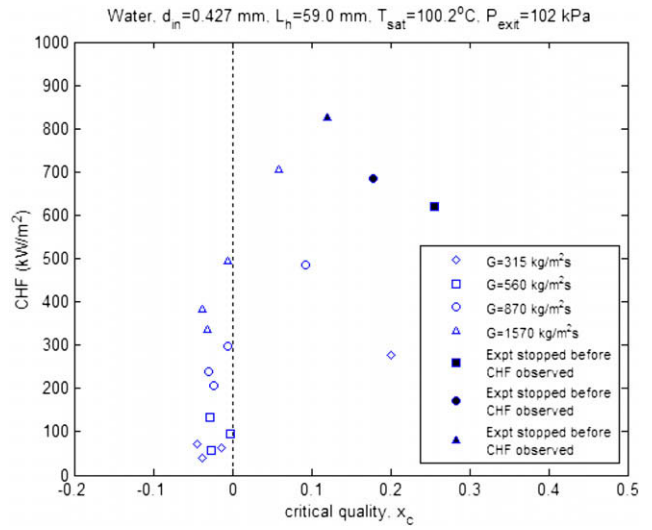

Fig. 13. Effect of exit quality on CHF for d_{in} = 0.427 mm and P_{exit} = 102 kPa.

Detailed results for the effect of exit quality on CHF for d_{in} = 0.427 mm are presented in Fig. 13. Note that in Fig. 13, the CHF first decreases with an increase in quality in the subcooled region, but with a further increase in quality (near zero quality and above), the CHF is found to have an increasing trend with quality. Much higher values of CHF are found in the region close to saturation when compared to the high subcooled region. With still further increases in heat flux/exit quality, the CHF condition did not occur even when the wall superheat ($\Delta T_{sat} = T_w - T_{sat}$) reached about 40–60 °C; the wall temperature increased essentially linearly with increases in heat flux. At this point, the experiment was terminated to save the test section. Therefore, very few data could be obtained in the saturation region. The results for the exit quality are consistent with the trends observed for the variation of CHF with inlet subcooling.

In the case of test section having inside diameter of 0.700 mm, a similar trend for inlet subcooling and exit quality was observed for experiments conducted with both heated lengths (L_h = 70.7 and 96.0 mm).

With tube diameter of 0.286 mm data trends for inlet subcooling and exit quality were very similar to that observed for d_{in} = 0.427 and 0.700 mm at higher mass fluxes. However, for G = 320 kg/m^{2}s, much higher critical qualities were found (as high as 0.9) in the saturated region for P_{exit} = 102 kPa (Fig. 15) and maximum critical quality of about 0.6–0.7 was attained at the lower exit pressure of 26 kPa. There are two interesting cases observed in the data:

1. Case I (Fig. 14) – CHF seems to initially decrease with a reduction in inlet subcooling in the higher absolute value of the negative critical quality region. However, the decrease is not too evident in some of the data because the negative critical quality band is narrow. More data at still higher inlet subcoolings over a wider range would be able to provide more insight into this speculation. With further decrease in inlet subcooling, CHF increased (similar to observations for d_{in} = 0.427 and 0.700 mm), and finally (when very low inlet subcoolings approached), CHF had a decreasing trend with quality (similar to that in conventional tubes) where the flow seems to be annular as discussed in a later section on flow maps.
2. Case II – CHF seems to initially decrease with a reduction in inlet subcooling at higher negative critical quality. With further decrease in inlet subcooling, CHF increased (up to low inlet

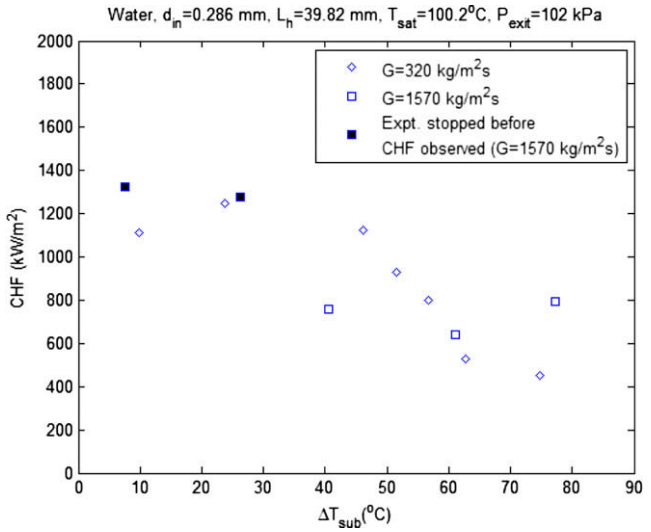

Fig. 14. Effect of inlet subcooling on CHF (d_{in} = 0.286 mm, L_h = 39.82 mm, and P_{exit} = 102 kPa).

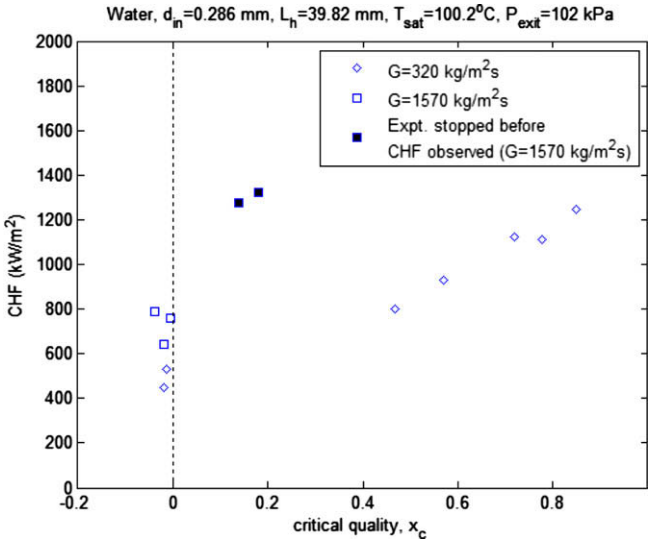

Fig. 15. Effect of exit quality on CHF (d_{in} = 0.286 mm, L_h = 39.82 mm, and P_{exit} = 102 kPa).

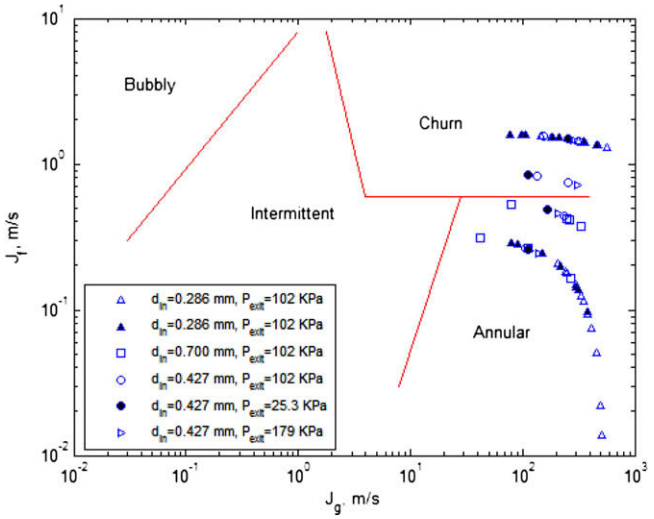

Fig. 16. Water data flow patterns using flow-pattern map of Hassan et al. [28].

subcoolings). The decreasing trend of CHF with further decrease in inlet subcooling at very low subcoolings is not obvious or present (similar to Fig. 12) as the data fall in the transition regime between churn and annular flow.

These data are not in apparent agreement with some other data that exist for CHF in microchannels. For example, the data by Wojtan et al. [13] show the CHF to be affected by exit quality, but only a small influence of inlet subcooling is observed. However, they state that measurements with larger inlet subcoolings were not possible, and so the data are for subcooling ranging only from 4.5 to 12 °C. They claim the observation to be in good agreement with the results of Qu and Mudawar [9] for parallel microchannels. However, Qu and Mudawar observed parallel channel instability (vapor back flow) as the CHF was approached, resulting in a diminished influence of inlet subcooling as vapor mixed with the subcooled inlet fluid in the plenum. Their data showed hardly any influence of inlet subcooling.

The increase in CHF from subcooled to the saturated region (as observed in the data) was also seen by Nariai et al. [5] in their studies on CHF in minitubes (1–3 mm inside diameter) but with much higher mass fluxes (7000–11,000 kg/m^{2}s). The maximum exit quality in their data was 0.05. Bergles et al. [27] reported similar findings for flow of water through a 2.38 mm tube with a mass flux of 1350 kg/m^{2}s. They found the CHF to increase from subcooled to the saturated region, but at qualities above 0.4, the CHF had a conventional decreasing trend (dryout type behavior). Similarly, the data from Wojtan et al. [13] showed a decreasing trend of CHF with quality ($x > 0.4$), but no data were available at lower qualities, and thus, no comments can be made about the discontinuity from subcooled to saturated region.

During the present experiments it was not possible to visualize the flow to determine the flow patterns. The data were mapped using the flow pattern maps available for microchannels to assess the flow condition at the instance of the CHF condition. First the water CHF data are mapped using the flow pattern map of Hassan et al. [28]. This is a universal flow map developed for horizontal microchannels of diameter less than 1.0 mm. The effects of surface tension are more significant in microchannels and this flow map characterizes the flow regimes in two major categories: the surface tension (bubbly, plug, and slug flow) and inertia dominated flow regimes (churn and annular). The redefined transition boundaries gave a good approximation of flow regime transitions when Hassan et al. compared the flow map with the previous studies that were conducted in microchannels. The water CHF data of the present study mapped using the Hassan et al. flow map are shown in Fig. 16 and indicate the flow-type at the instance of the CHF condition.

The superficial liquid (J_f) and superficial gas velocities (J_g) were calculated as

$$J_f = \frac{G(1 - x_c)}{\rho_f} \tag{2}$$

$$J_g = \frac{Gx_c}{\rho_g} \tag{3}$$

The following observations are made from this flow regime map:

(a) Most of the data fall in the churn flow, churn–annular transition or annular flow very close to the transition zone.
(b) Almost all of the data where the experiment had to be stopped to prevent destruction of the test section fell in the churn flow regime.
(c) Most of the data from the tube diameters of 0.427 and 0.700 mm were either in the churn or the churn–annular transition zone. The churn flow is characterized by a highly irregular interface with oscillatory flow of the liquid. With increase in quality in the saturated region, more vapor is generated, and it is possible that the waves are stabilized due to the high vapor. This might be a possible reason for increase in CHF with quality during the transition as observed in all the saturated CHF data for the tube diameters of 0.427 and 0.700 mm.
(d) Some of the data for tube diameter of 0.286 mm were in annular flow, with the remaining in churn or churn–annular regime. It is interesting to see that the data for this tube diameter far away from the churn–annular transition line correspond to those at very high qualities where the CHF has a decreasing trend with inlet subcooling and CHF is almost constant or decreases slightly with exit quality. The flow then could be an annular flow exhibiting dryout type behavior. For all other data points (in churn flow as well as churn–annular transition) and even those in annular flow closer to transition, the flow might still be churn/intermittent and a similar behavior as observed in other tube diameters is expected where the CHF increases with quality. For

tube of 0.286 mm diameter, annular flow far away from transition is observed at very high qualities where we would expect behavior similar to conventional tubes.

Since the present study involves boiling heat transfer, the data were also mapped using a flow-pattern map developed for evaporative flow in microchannels by Revellin and Thome [29]. This flow map classifies the flow into three regimes – isolated bubble regime, coalescing bubble regime and the annular regime and is not universal. A new flow map is needed for every diameter, pressure, and heat flux. Also, it is recommended that this flow map be used by evaluating properties at the inlet conditions and the range of application is limited to the range of parameters for which the flow map study was conducted. The Revellin and Thome study was conducted for two refrigerants R-134a and R-245fa and inlet subcoolings 2–15 °C, T_{sat} = 26, 30, and 35 °C, G = 210–2094 kg/m^{2}s, d_{in} = 0.509 and 0.790 mm, and L_h = 20–70 mm. The CHF experiments with R-123 are closer to this parametric range than those conducted with water as the working fluid. The calculations for critical quality in this study are based on the exit pressure. Even for the data having very high pressure drops, for both water and R-123, at higher qualities, the difference in the values of qualities based on inlet and exit pressures is not too significant. For example, in case of water CHF data for d_{in} = 0.286 mm, P_{exit} = 26 kPa and ΔP_T = 74.7 kPa, x_c based on exit pressure is 0.59 and based on inlet pressure is 0.53. For R-123, in case of d_{in} = 0.286 mm, P_{exit} = 165 kPa and ΔP_T = 84.0 kPa, x_c based on exit pressure is 0.55 and based on inlet pressure is 0.46. Therefore, both water and R-123 CHF data were mapped using the Revellin and Thome map (with the changes as mentioned above) showing only the transition from coalescing bubble region to annular region to map the present CHF data (water and R-123), otherwise a new flow map would be needed for each CHF data point.

In Fig. 17, the solid lines indicate the flow pattern transitions from coalescing bubble (CB) to annular flow (A) regime using Revellin and Thome correlation and the symbols indicate the experimental CHF data points. This flow map predicts that none of the CHF data points are in the annular region and data points for tube diameters of 0.7 and 0.427 mm are far away from the transition line. But, as pointed out earlier, it is not clear if any of such CHF data exist in the isolated bubble regime or in the isolated bubble–coalescing bubble transition regime. However, the Hassan et al. flow map predicts annular flow for some of the experimental CHF data points. Again, it should be noted that the experimental parameters in the CHF studies with water are very different from those that are used to obtain the Revellin and Thome flow map.

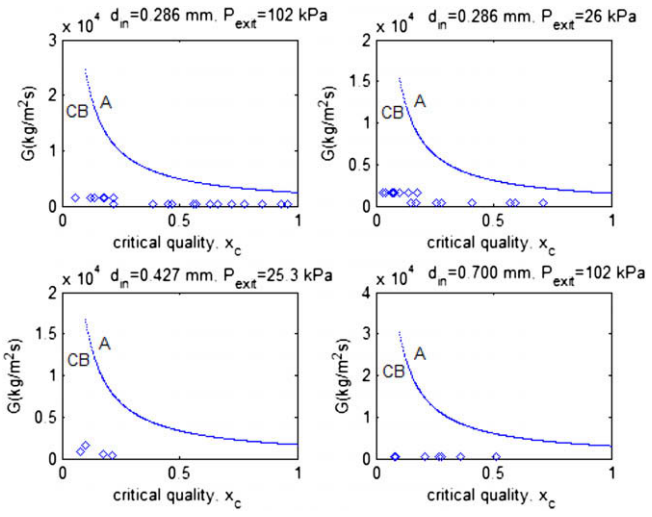

Fig. 17. Water CHF data mapped using flow pattern map of Revellin and Thome [29].

Thus, based on the conclusions drawn from the data and the flow regime map, the behavior of CHF with quality can be summarized in the Fig. 18 in which the behavior of CHF with quality is marked by two transition points: Transition A, which might depend on the net vapor generation (dealt in Part II of the paper), and Transition B, which depends on the establishment of annular flow in the tube. These transition points are clearly functions of the operating parameters, and based on the chosen condition, one or the other type of behavior is seen. The CHF condition between these two transition points is governed by a transitional behavior as the mechanism changes from (probably) a DNB-type behavior in the subcooled region to a dryout behavior at higher qualities.

The relationship between CHF and inlet subcooling or CHF and exit quality for the R-123 data obtained in this study is not simple, similar to that observed in the water CHF data. The R-123 CHF data were also mapped on the flow regime map developed by Hassan et al. [28] for flow in circular tubes below 1.0 mm diameter and are shown in Fig. 19. The following observations are made:

(a) Most of the data for d_{in} = 0.430 and 0.700 mm fall in the intermittent zone. The intermittent flow regime regroups all the slug and plug flows, as well as the transition flow occurring in the vicinity of the intermittent region.
(b) Almost all of the experimental data for d_{in} = 0.286 mm lie in the annular regime but very close to the transition between the slug and annular flow. Hence, for these data it cannot be predicted if the flow is "completely annular".

Also, as was studied with water, the data were mapped using the flow pattern map of Revellin and Thome [29] and is depicted in Fig. 20. This map predicts that most of the data for tube diameter of 0.286 mm is in the coalescing bubble (CB) regime close to the transition and some data are in the annular (A) flow regime. Some data for tube diameters of 0.430 and 0.700 mm appear to be in the coalescing bubble regime and none are in the annular flow. The flow predictions using the Revellin and Thome flow map are closer to those predicted by Hassan et al. for R-123 than is the case for water. It should be noted that the experimental parameters for water are very different from those used in the Revellin and Thome flow map.

For the R-123 data with d_{in} = 0.430 and 0.700 mm, the exit pressure was 168 kPa which corresponds to the saturation temperature of 42.5 °C. The range of inlet subcooling was from 1 to 14 °C and the critical qualities at the exit were from 0.2 to 0.35 for d_{in} = 0.430 mm and 0.05 to 0.2 for d_{in} = 0.700 mm. Thus, the data were obtained in a limited range. The CHF slightly increased or

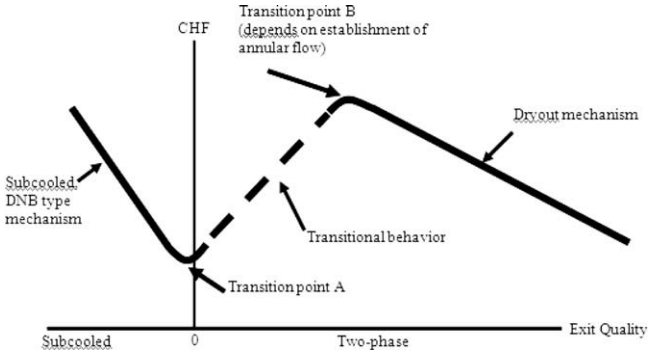

Fig. 18. Speculations on the trends of CHF with exit quality.

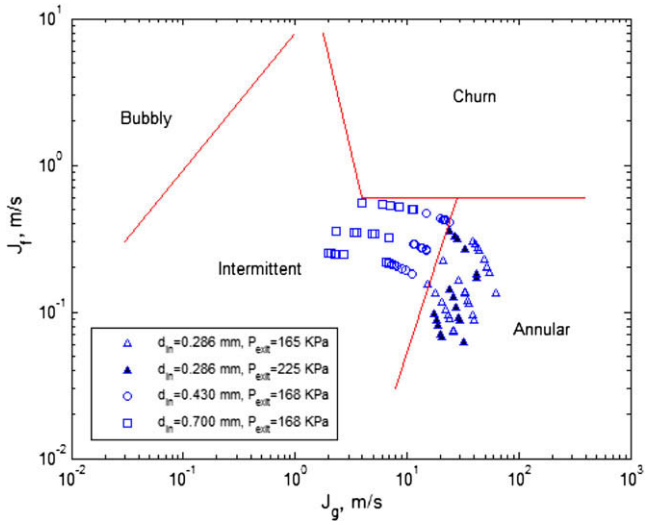

Fig. 19. Flow patterns for R-123 using Hassan et al. [28] flow map.

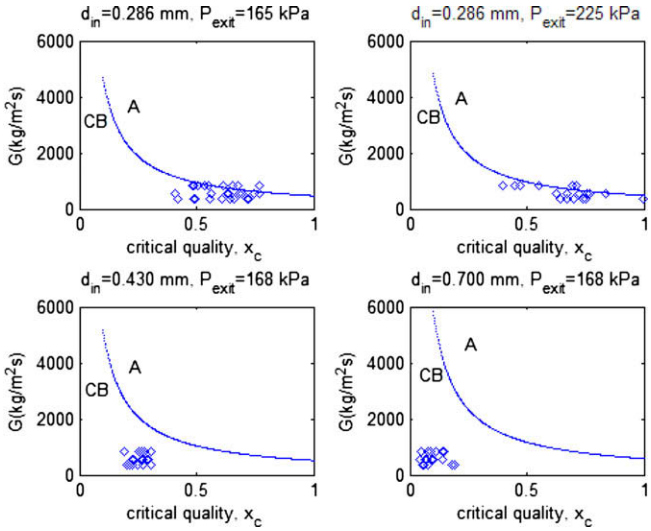

Fig. 20. Flow patterns for R-123 using Revellin and Thome [29] flow map.

was fairly constant with a reduction in inlet subcooling for both the tube diameters, which is contrary to that observed in conventional sized channels and is shown for 0.700 mm diameter in Fig. 21.

Experiments conducted with test section of inside diameter 0.286 mm show that the CHF first increases with reduction in inlet subcooling, but starts to decrease as the inlet temperature of the fluid approaches the saturation temperature (Fig. 22). The data points which correspond to the decreasing trend of CHF with inlet subcooling are farther away from the intermittent–annular transition line. These data not only show a decrease in the CHF value but also are marked by a lower value of critical quality. This suggests that as the fluid inlet temperature approaches the saturation temperature, the annular flow is triggered at lower qualities. But data points closer to the annular–intermittent transition show an increase in CHF with inlet subcooling and the trends exhibit an increase in critical quality (Fig. 23) as the inlet temperature is raised (subcooling is lowered).

4.3.3. Effect of heated length on CHF

CHF studies with water were conducted at different heated lengths of 21.66, 39.82, and 57.6 mm for the tube diameter of 0.286 mm. The results for P_{exit} = 102 kPa are shown in Fig. 24 for the mass flux of 320 kg/m^{2}s and five different conditions of inlet subcoolings. The results show an inverse dependence of CHF on heated length.

For the R-123 data as well, the CHF is found to decrease with an increase in heated length at a fixed value of inlet subcooling as seen in Fig. 25 for tube diameter of 0.430 mm. When the same data are plotted against the exit quality (Fig. 26), it is observed that the CHF decreases with an increase in heated length at a fixed exit quality, unlike large tube diameters. This behavior is similar to that seen in the water CHF data of the present study. The experiments with d_{in} = 0.286 and 0.700 mm also show the inverse relationship of CHF with heated length for fixed inlet subcooling. Fig. 27 depicts this relationship for d_{in} = 0.286 mm with three different heated lengths for a mass flux of G = 825 kg/m^{2}s. The data at other mass fluxes (375 and 530 kg/m^{2}s) show a similar trend.

4.3.4. Effect of exit pressure on CHF

For water, the CHF increases with an increase in exit pressure for a constant value of inlet subcooling. This behavior for d_{in} = 0.286 mm is depicted in Fig. 28 for the heated length of

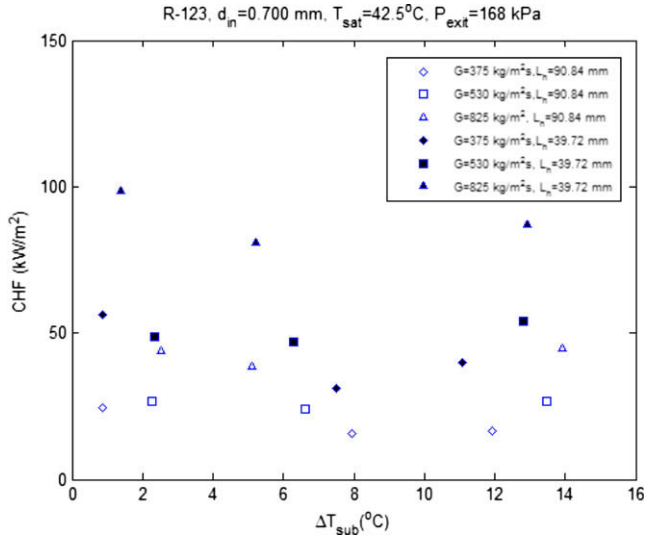

Fig. 21. Effect of inlet subcooling on CHF for R-123 with d_{in} = 0.700 mm.

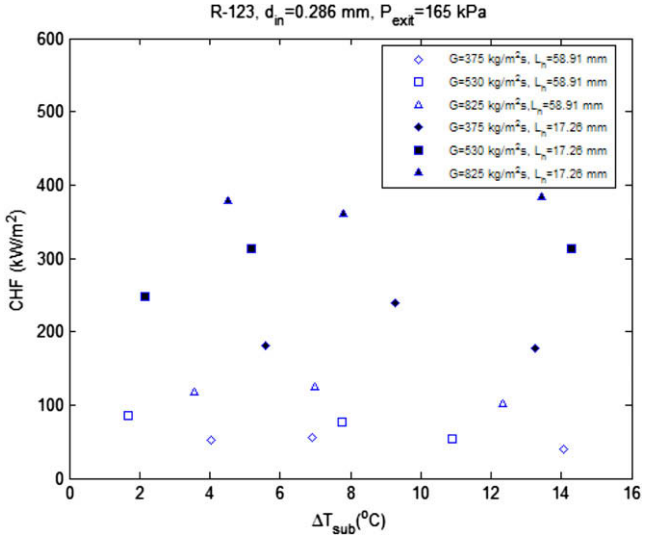

Fig. 22. Effect of inlet subcooling on CHF for R-123 with d_{in} = 0.286 mm.

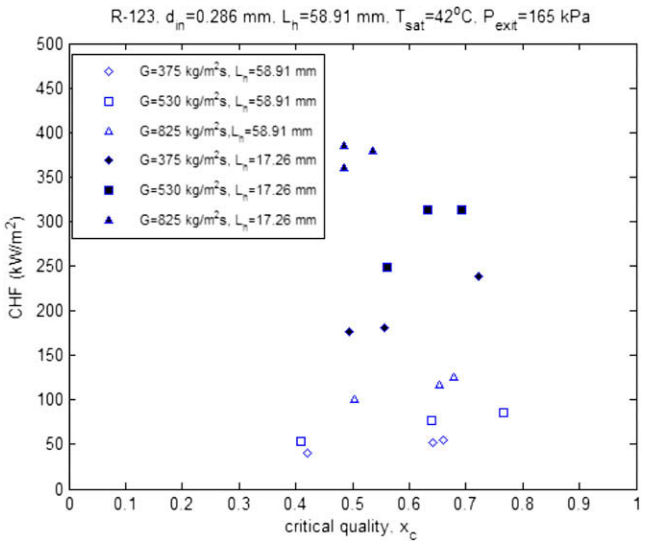

Fig. 23. Effect of exit quality on CHF for R-123 with d_{in} = 0.286 mm.

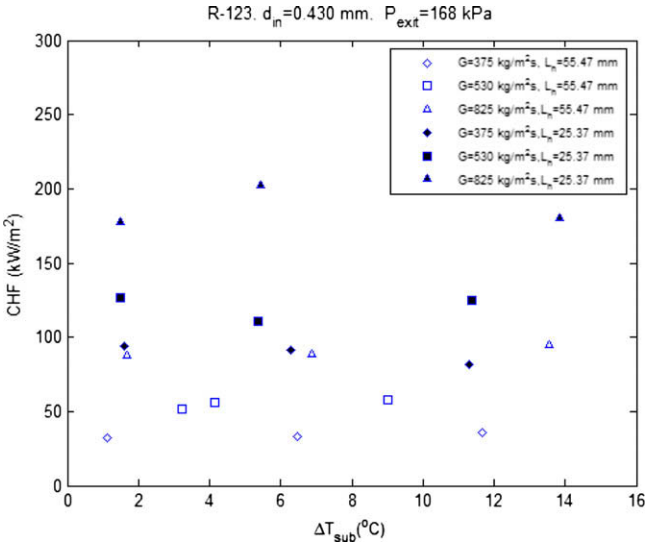

Fig. 25. Effect of heated length on CHF for d_{in} = 0.430 mm at fixed inlet subcoolings.

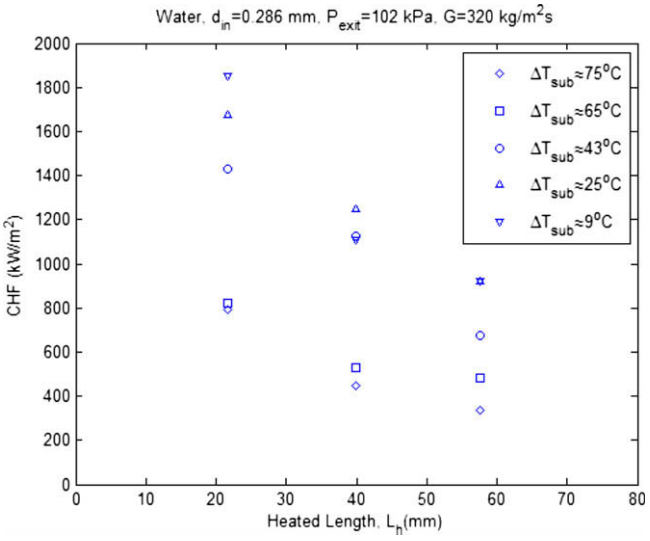

Fig. 24. Effect of heated length on CHF (d_{in} = 0.286 mm, G = 320 kg/m^{2}s, P_{exit} = 102 kPa).

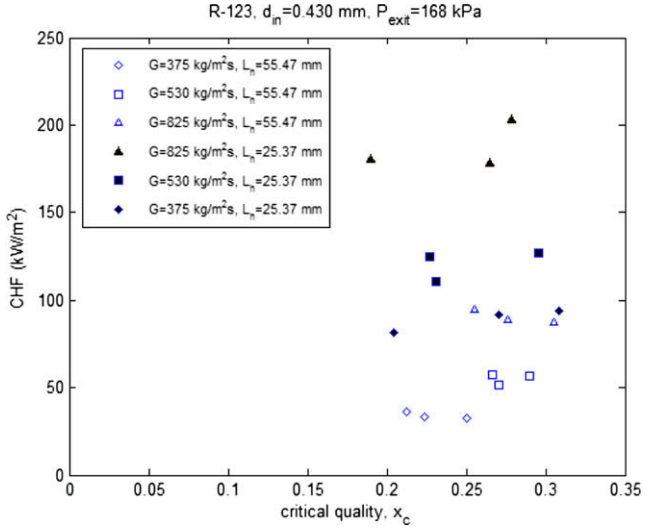

Fig. 26. Effect of heated length on CHF for d_{in} = 0.430 mm at fixed exit quality.

57.62 mm. Results for d_{in} = 0.427 mm also show that the CHF is pressure dependent and increases with an increase in exit pressure.

CHF studies were conducted by Wojtan et al. [13] for R-134 in tube of inside diameter 0.5 mm at two different saturation temperatures of 30 and 35 °C. They found that there was hardly any difference in CHF values for tests at these two saturation temperatures below mass fluxes of 1000 kg/m^{2}s, but for higher values of mass flux, the CHF increased with saturation temperature (increase in pressure). Experimental studies by Kosar and Peles [17] in silicon-based parallel microchannel heat sink over exit pressures from 227 to 520 kPa showed that the CHF increased with increase in exit pressure up to about 315 kPa for a range of mass fluxes and had a decreasing trend with increase in exit pressures beyond 315 kPa. Thus, they observed a maximum in the CHF value in the experiments conducted over a range of exit pressures.

Studies were conducted with R-123 at two different exit pressures of 165 and 225 kPa for the test section with inside diameter of 0.286 mm for two different heated lengths of 17.26 and 58.91 mm. It can be seen from Fig. 29 that the effect of pressure on CHF is not significant. However, the water CHF data did show a large influence of pressure on CHF. It should be noted that the water experiments were conducted over a much larger range of density ratios than those for R-123 (Table 2).

4.3.5. Effect of diameter on CHF

The water CHF data for the three different tube diameters are given in Fig. 30. The data compared are for a mass flux of about 320 kg/m^{2}s, $L_h/d \approx 139$, and exit pressure close to atmospheric. The CHF increased substantially with a reduction in tube diameter to 0.286 mm from 0.427 mm. The differences in the CHF values for tube diameters of 0.427 and 0.700 mm are not substantial and the CHF values seem to be higher for d_{in} = 0.700 mm compared to 0.427 mm in the negative quality region. It is worth noticing that most of these data are very close to x = 0, with couple of data points from d_{in} = 0.700 mm almost at x = 0. As pointed out earlier, CHF increases from the subcooled to the saturation region and since these data points are so close to the saturation, the inverse dependence is not apparent. But, looking at the CHF values in the saturation region, CHF for d_{in} = 0.427 mm is about 290 kW/m^2 (at $x \approx 0.2$) and that for d_{in} = 0.700 mm is about 140 kW/m^2 (at $x \approx 0.09$).

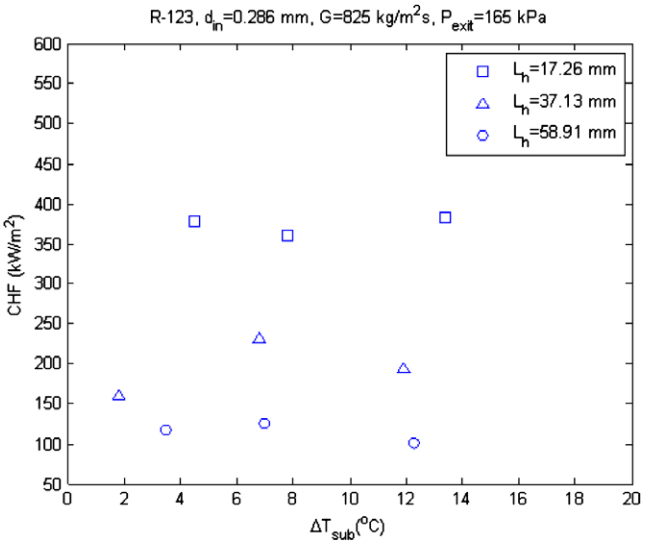

Fig. 27. Effect of heated length on CHF for R-123; d_{in} = 0.286 mm, G = 825 kg/m^{2}s.

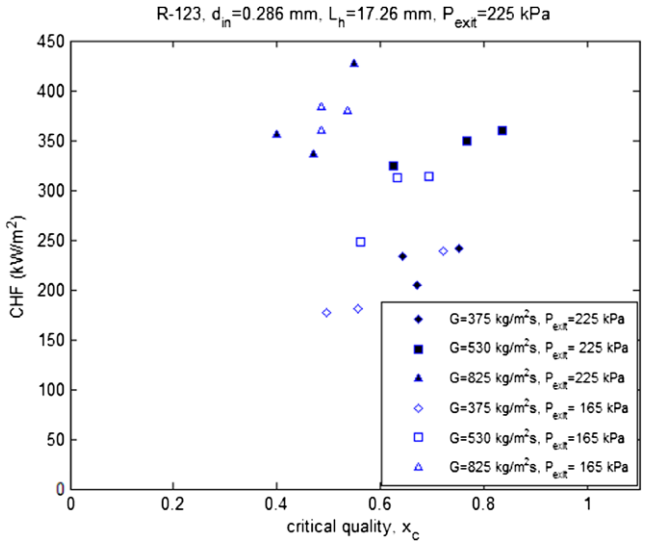

Fig. 29. Effect of exit pressure on CHF for d_{in} = 0.286 mm, L_h = 17.26 mm.

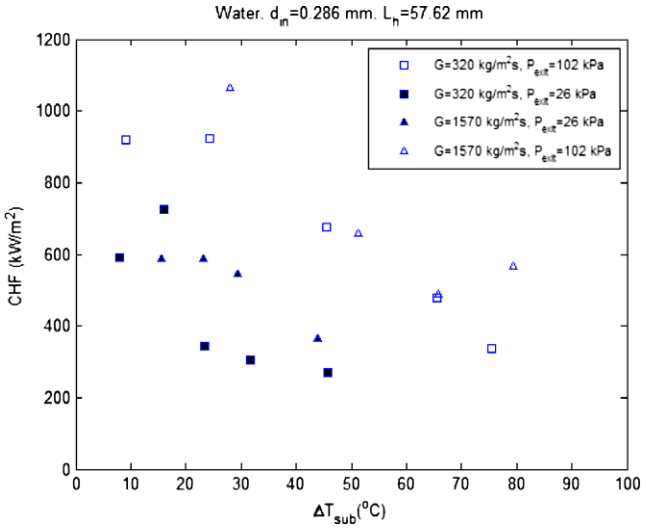

Fig. 28. Effect of exit pressure on CHF (d_{in} = 0.286 mm, L_h = 57.62 mm).

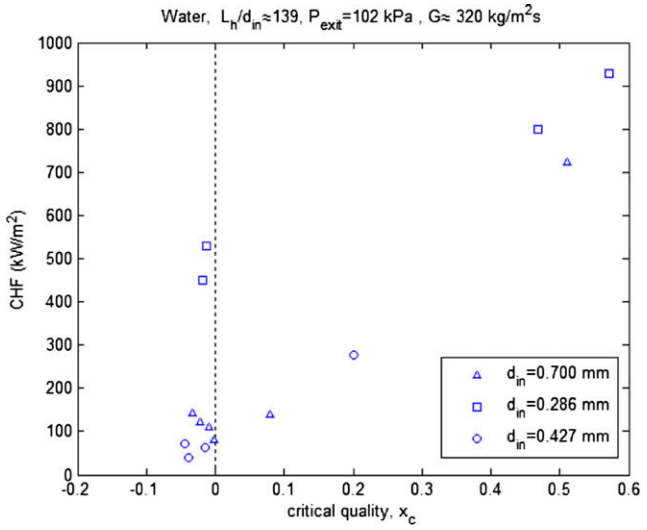

Fig. 30. Effect of tube diameter on CHF ($L_h/d_{in} \approx 139$, $G \sim 320$ kg/m^{2}s, P_{exit} = 102 kPa).

Studies with R-123 conducted with three different diameter tubes show that the CHF has an inverse dependence on diameter. Fig. 31 is plotted for the inside diameters of 0.286, 0.430, and 0.700 mm for similar P_{exit}, L_h/d_{in}, and ΔT_{sub}. It is evident that the CHF decreases with an increase in diameter over the entire range of mass fluxes included in the study. This dependence is similar to that observed for the CHF experiments with water except that the CHF values for tube diameters of 0.427 mm are higher than 0.700 mm as much higher critical qualities were obtained with R-123 (x_c = 0.2–0.35 for d_{in} = 0.430 mm and x_c = 0.05–0.2 for d_{in} = 0.700 mm).

5. Conclusions

The following conclusions can be drawn from the present studies:

- For the single-phase studies in microtubes, with R-123 and water, the pressure drop characteristics were consistent with conventional sized channels in laminar flow, but there was a marked inconsistency in the heat transfer characteristics where *Nu* was underpredicted at lower *Re* and overpredicted at higher *Re*. Similar observations have been made by other researchers and a definite reason for this disagreement in microchannels is not yet established.
- Because of a high pressure drop upstream of the test section, a stable flow during the CHF experiments made possible acquiring stable CHF data. The critical heat flux condition in experiments with water, as well as R-123, was marked by a sharp rise in wall temperature towards the exit of the heated section. The wall superheat at the onset of CHF for R-123 tests varied from about 11 to 35 °C. For most of the water CHF tests, the wall superheat was between 3 and 25 °C, but for data at lower inlet subcoolings very high wall superheats (50–60 °C) were seen before the characteristic CHF occurred. In such tests, wall temperatures increased linearly with heat flux until the CHF condition was attained. Still, for some other tests with water at very low inlet subcoolings, this increasing trend of wall superheat with heat flux continued, and experiments had to be stopped before the characteristic CHF could be observed to save the test section for further experiments. Such behavior was not seen in R-123 data.

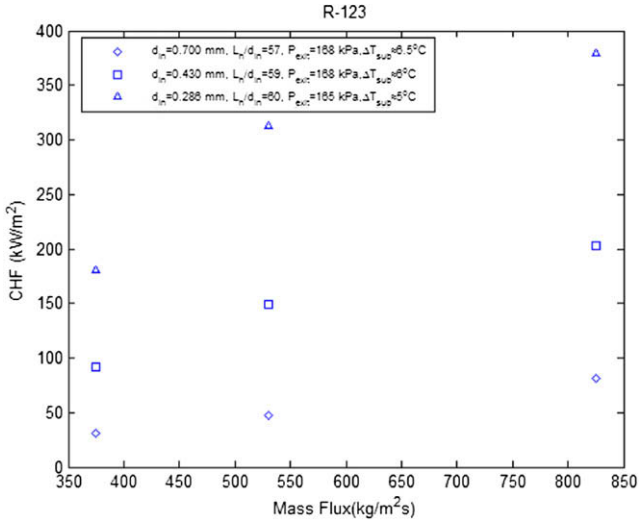

Fig. 31. Effect of diameter on CHF for R-123.

In microchannels, at higher vapor qualities it is likely that a stable vapor core is established (bubble grows to the channel size very quickly), typical bubbly flow is suppressed, and evaporation at the liquid film vapor core is the dominant heat transfer mechanism. Such flow pattern has been observed by Thome et al. and could be a possible reason for wall temperatures to increase linearly with heat flux from single-phase region until the CHF, and the typical change in slope of ΔT_{sat} versus q'' during boiling (boiling plateau) is suppressed. Jiang et al. had observed such wall temperature behaviors as well. In the present study, with water and R-123, similar wall temperature response with heat flux (linearly increasing) is more pronounced in experiments conducted with very low inlet subcoolings.

The data from this study were mapped using the flow pattern maps developed by Hassan et al. and by Revellin and Thome for microtubes. Most of the water CHF data lie in the churn, churn–annular transition and annular regions close to the transition whereas the R-123 data are in the slug, slug–annular and annular regions. The data for water have high superficial liquid velocities and, hence, likely to exhibit a churn type behavior as opposed to the slug behavior in the R-123 data.

From the extensive experiments conducted in this study, it is seen that flow patterns have a strong influence on the way different operating parameters affect the CHF condition. Previous studies on CHF have not thoroughly investigated the effect of the different operating parameters. Such parametric effects on CHF were analyzed in this study for water and R-123, and the following observations were made:

- The increasing trend of CHF with mass flux is in general agreement with other researchers on CHF in microchannels. In the present data, for saturated conditions, the CHF is found to increase with mass flux at fixed exit quality and is contrary to that found in conventional sized tubes. In conventional sized tubes, increasing mass flux increases the CHF in the subcooled region because of increased convective effects, whereas in the saturated region, increasing the mass flux decreases the CHF at a given quality. This is a result of increased entrainment which accompanies increasing mass flux in the annular flow regime. The data here similarly show an increasing trend of CHF with mass flux for a fixed value of inlet subcooling in the subcooled region and also have the same trend in the saturated region (refer to the sub-section on the effect of exit quality on CHF). This might indicate that the flow regime in not "fully" annular in the sense that entrainment in the vapor core is not too significant. Such comparisons of mass flux effects at fixed exit quality in the saturation region have not been done by other researchers. This contrary behavior could be because the data are taken for comparatively lower mass fluxes and pressures than are available for large-sized tubes. In this study, two types of flow patterns, churn and annular, exist in positive quality CHF conditions. The slug type of flow pattern during R-123 tests shows mainly subcooled CHF behavior. It is possible that the wavy interface during churn flow is more stable at higher vapor velocities (for the same quality) leading to an increase in CHF with mass flux. Also, for the CHF data with annular flow, since such flows are triggered at lower heat fluxes, it could be likely that initially large amount of droplets are broken off into vapor core and as flow advances, the liquid droplets get deposited back on the liquid film increasing its thickness, and this rate of deposition could be higher for higher mass flux at the same quality inducing higher CHF values.
- The data exhibit a complex behavior of CHF with exit quality. For the experiments conducted with water most of the data are in the subcooled region with some being in the saturated region. The CHF decreased with an increase in quality in the subcooled region, but as qualities approached zero, this trend was reversed, and the CHF increased with quality into the saturated region. Similar findings were reported by Nariai et al. and Bergles et al. in minitubes.

Based on the data obtained in this study, Part II of the paper will deal with the comparison of the data with the existing CHF correlations (micro/macrochannels). A new correlation will be proposed to predict CHF based on the trends obtained in this study. Also, the unique behavior of the CHF with exit quality will be looked into detail to see if the point of net vapor generation (PNVG) could be one of the transition points for the change in behavior from the subcooled to the saturated region.

Acknowledgments

The support of the National Science Foundation with Grant No. CTS 0245642 and of Rensselaer Polytechnic Institute is gratefully acknowledged. This work is supported in part by the Office of Naval Research (ONR) under the Multidisciplinary University Research Initiative (MURI) Award GG10919.

References

[1] S. Kakac, H. Liu, Heat Exchangers: Selection, Rating and Thermal Design, CRC Press, 1998. pp. 903–904 (Chapter 9).
[2] C.L. Vandervort, A.E. Bergles, M.K. Jensen, An experimental study of critical heat flux in very high heat flux subcooled boiling, Int. J. Heat Mass Transfer 37 (Suppl. 1) (1994) 161–173.
[3] G.P. Celata, M. Cumo, A. Mariani, Burnout in highly subcooled water flow boiling in small diameter tubes, Int. J. Heat Mass Transfer 36 (1993) 1269–1285.
[4] G.P. Celata, M. Cumo, A. Mariani, Geometrical effects on the subcooled flow boiling critical heat flux, Rev. Générale Thermique 36 (1997) 807–814.
[5] H. Nariai, F. Inasaka, K. Uehara, Critical heat flux in narrow tubes with uniform heating, Trans. Jpn. Soc. Mech. Eng. 54 (1988) 1406–1410.
[6] A.E. Bergles, W.M. Rohsenow, Forced-convection surface-boiling heat transfer and burnout in tubes of small diameter, Contract AF 19(604)-7344 Report, Department of Mechanical Engineering, Massachusetts Institute of Technology, 1962.
[7] G.M. Roach Jr., S.I. Abdel-Khalik, S.M. Ghiaasiaan, M.F. Dowling, S.M. Jeter, Low flow critical heat flux in heated microchannels, Nucl. Sci. Eng. 131 (1999) 411–425.
[8] G.M. Lazarek, S.H. Black, Evaporative heat transfer, pressure drop and critical heat flux in a small vertical tube with R-113, Int. J. Heat Mass Transfer 25 (1982) 945–960.

[9] W. Qu, I. Mudawar, Measurement and correlation of critical heat flux in two-phase micro-channel heat sinks, Int. J. Heat Mass Transfer 47 (2004) 2045–2059.
[10] W. Yu, D.M. France, M.W. Wambsganss, J.R. Hull, Two-phase pressure drop, boiling heat transfer, and critical heat flux to water in a small-diameter horizontal tube, Int. J. Multiphase Flow 28 (2002) 927–941.
[11] A.M. Lezzi, A. Niro, G.P. Beretta, Experimental data on CHF for forced convection water boiling in long horizontal capillary tubes, in: Proceedings of the 10th International Heat Transfer Conference, vol. 7, Rugby, UK, 1994, pp. 491–496.
[12] L. Jiang, M. Wong, Y. Zohar, Phase change in microchannel heat sinks with integrated temperature sensors, J. Microelectromech. Syst. 8 (1999) 358–365.
[13] L. Wojtan, R. Revellin, J.R. Thome, Investigation of saturated critical heat flux in a single uniformly heated microchannel, Exp. Thermal Fluid Sci. 30 (2006) 765–774.
[14] A.P. Roday, T. Borca-Tasçiuc, M.K. Jensen, The critical heat flux condition with water in a uniformly heated microtube, J. Heat Transfer 130 (2008) 012901-1–012901-10.
[15] A.E. Bergles, S.G. Kandlikar, On the nature of critical heat flux in microchannels, J. Heat Transfer 127 (2005) 101–107.
[16] A. Koşar, C.-J. Kuo, Y. Peles, Suppression of boiling flow oscillations in parallel microchannels by inlet restrictors, J. Heat Transfer 128 (2006) 251–260.
[17] A. Koşar, Y. Peles, Critical heat flux of R-123 in silicon-based microchannels, J. Heat Transfer 129 (2007) 844–851.
[18] W.K. Kuan, S.G. Kandlikar, Critical heat flux measurement and model for efrigerant-123 under stabilized flow conditions in microchannels, in: Proceedings of IMECE 2006, IMECE2006-13310, 2006 ASME International Mechanical Engineering Congress and Exposition, Chicago, IL, USA, November 5–10, 2006.
[19] C.H. Oh, S.B. Englert, Critical heat flux for low flow boiling in vertical uniformly heated thin rectangular channels, Int. J. Heat Mass Transfer 36 (1993) 325–335.
[20] M.B. Bowers, I. Mudawar, High flux boiling in low flow rate, low pressure drop mini-channel and micro-channel heat sinks, Int. J. Heat Mass Transfer 37 (1994) 321–332.
[21] S.J. Kline, F.A. McClintock, Describing uncertainties in single sample experiments, Mech. Eng. 75 (1953) 3–8.
[22] A.P. Roday, Study of the critical heat flux condition in microtubes, Ph.D. thesis, Rensselaer Polytechnic Institute, Troy, NY, 2007.
[23] G.P. Celata, M. Cumo, M. Guglielmi, G. Zummo, Experimental investigation of hydraulic and single-phase heat transfer in 0.13-mm capillary tube, Microscale Thermophys. Eng. 6 (2002) 85–97.
[24] X.F. Peng, G.P. Peterson, Convective heat transfer and flow friction for water flow in microchannel structures, Int. J. Heat Mass Transfer 39 (1996) 2599–2608.
[25] G.P. Celata, N. Ksagi, Preface, Int. J. Heat Fluid Flow 28 (2007) 1.
[26] A. Koşar, C.-J. Kuo, Y. Peles, Reduced pressure boiling heat transfer in rectangular microchannels with interconnected reentrant cavities, J. Heat Transfer 127 (2005) 1106–1114.
[27] A.E. Bergles, R.F. Lopina, M.P. Fiori, Critical-heat-flux and flow-pattern observations for low-pressure water flowing in tubes, J. Heat Transfer (1967) 69–74.
[28] I. Hasaan, M. Vaillancourt, K. Pehlivan, Two-phase flow regime transitions in microchannels: a comparative experimental study, Microscale Thermophys. Eng. 9 (2005) 165–182.
[29] R. Revellin, J.R. Thome, A new type of diabatic flow pattern map for boiling heat transfer in microchannels, J. Micromech. Microeng. 17 (2007) 788–796.